JCI The Journal of Clinical Investigation

On the Uptake of Materials by the Intact Liver THE CONCENTRATIVE TRANSPORT OF RUBIDIUM-86

Carl A. Goresky, … , Glen G. Bach, Brita E. Nadeau

J Clin Invest. 1973;52(5):975-990. https://doi.org/10.1172/JCI107299.

Research Article

In this study we use the multiple indicator dilution technique to outline the kinetic mechanisms underlying the uptake of rubidium, a cation which, in the steady state, is concentrated by hepatic parenchymal cells. We inject a mixture of ^{51}Cr-labeled red blood cells (a vascular reference substance), ^{22}Na (which is confined to the extracellular space, the expected extravascular distribution space for rubidium, in the absence of cellular uptake), and ^{86}Rb into the portal vein and obtain normalized outflow patterns, expressed as outflowing fractions of each injected mass per milliliter vs. time. The labeled red cell curve rises to the highest and earliest peak and decays rapidly. That for labeled sodium rises to a later and lower peak, and decays less rapidly. Its extrapolated recovery is equal to that for the red cells. The observed ^{86}Rb curve consists of two parts: an early clearly defined peak of reduced area, related to the ^{22}Na peak in timing; and a later tailing, obscured by recirculation, so that total outflow recovery cannot be defined (even though it would be expected to be the same). We model the concentrative uptake of ^{86}Rb and find two corresponding outflow fractions: throughput material, which sweeps past the cell surface as a wave delayed with respect to the vascular reference (tracer which has not entered cells); and exchanging material (tracer […]

On the Uptake of Materials by the Intact Liver

THE CONCENTRATIVE TRANSPORT OF RUBIDIUM-86

CARL A. GORESKY, GLEN G. BACH, and BRITA E. NADEAU

From the McGill University Medical Clinic in the Montreal General Hospital, and the Departments of Medicine and of Mechanical Engineering, McGill University, Montreal, Quebec, Canada

ABSTRACT In this study we use the multiple indicator dilution technique to outline the kinetic mechanisms underlying the uptake of rubidium, a cation which, in the steady state, is concentrated by hepatic parenchymal cells. We inject a mixture of ^{51}Cr-labeled red blood cells (a vascular reference substance), ^{22}Na (which is confined to the extracellular space, the expected extravascular distribution space for rubidium, in the absence of cellular uptake), and ^{86}Rb into the portal vein and obtain normalized outflow patterns, expressed as outflowing fractions of each injected mass per milliliter vs. time. The labeled red cell curve rises to the highest and earliest peak and decays rapidly. That for labeled sodium rises to a later and lower peak, and decays less rapidly. Its extrapolated recovery is equal to that for the red cells. The observed ^{86}Rb curve consists of two parts: an early clearly defined peak of reduced area, related to the ^{22}Na peak in timing; and a later tailing, obscured by recirculation, so that total outflow recovery cannot be defined (even though it would be expected to be the same). We model the concentrative uptake of ^{86}Rb and find two corresponding outflow fractions: throughput material, which sweeps past the cell surface as a wave delayed with respect to the vascular reference (tracer which has not entered cells); and exchanging material (tracer which has entered cells and later returns to the circulation). We find that the outflow form of the rubidium curve, the presence of both a relatively clearly defined throughput component and a relatively prolonged low-in-magnitude tailing, is consequent to the concentrative character of the transport mechanism, to the presence of an influx rate constant many times the efflux rate constant. The modeling which we develop is general, and has potential application in situations where transport is nonconcentrative.

Received for publication 3 February 1971 and in revised form 29 December 1972.

INTRODUCTION

In general, processes located in the membrane surrounding a cell produce and maintain an intracellular fluid distinctly different in composition from the surrounding medium. One of the major characteristics of most mammalian cells is the presence of a steady-state concentration of the cation potassium inside the cells which is many times that in the surrounding extracellular fluid. From the existence of both this large concentration gradient for potassium across the cellular membrane and a process allowing for the exchange of radioactive potassium-42 between the intracellular and extracellular pools, the presence of a net concentrative transport mechanism for potassium within the cell membrane may be inferred. Here we consider rubidium, an alkali metal which also belongs to group I in the periodic table and which has a diffusion coefficient which differs from that for potassium by less than 3% (1). Although there are some differences, the biological behavior of rubidium is remarkably similar to that of potassium: radioactive rubidium-86 disappears from the circulation at approximately the same rate as potassium-42 (2, 3); its single passage uptake by skeletal muscle is only slightly less than that of simultaneously administered tracer potassium (4); and after chronic administration of stable rubidium, the concentration ratio in skeletal muscle (cell/plasma) reaches and then finally exceeds the concomitant ratio for potassium when more than half the intracellular cation has become rubidium (5). In the liver, where the steady-state concentration ratio for potassium (tissue/plasma) is approximately 20, Love, Romney, and Burch have found that the rubidium-86 activity reaches a peak value an hour after intravenous injection, which is 30 times that of the concomitantly falling plasma level (6). The physical half-life of rubidium-86 is long enough that, unlike potassium-42, it is a convenient material to work with. Because of this convenience it has been widely

used as a tracer material representative of an intracellularly concentrated cation. We will continue to use it here, in the same sense.

The microcirculation of the liver is unique. The terminal elements of the circulation, the sinusoids, exhibit a discontinuous lining and there is no barrier between the surface of the liver cells and the lumen of the sinusoids. Substances entering the sinusoid and diffusing into the interstitial space (the space of Disse) therefore gain immediate access to the surface of the liver cells (7). In the present paper, we examine the behavior of rubidium, a substance for which the rate of uptake by hepatic cells is reasonably large. The experimental technique most appropriate for acquiring information concerning this process is the multiple indicator dilution technique, originally described by Chinard, Vosburgh, and Enns (8). It involves the injection into the blood stream of both a reference indicator and the substance under examination; the rapid serial collection of effluent hepatic venous samples; and the analysis of the samples to yield normalized outflow dilution patterns for each substance. The technique provides information in that time scale appropriate for defining the uptake rate for rubidium and it is nondestructive. To complement these data, we develop a kinetic hypothesis which relates the forms of the hepatic venous outflow dilution curves to the transport processes taking place at the surface of the cells; and utilize this hypothesis to derive from the rubidium-86 experiments numerical estimates of the parameters describing transport at the cell surface.

METHODS

General experimental procedures. In this study we use the rapid single-injection multiple indicator dilution technique in the dog. In each experiment we inject three labeled substances simultaneously: ^{51}Cr-labeled red cells as a vascular indicator, a substance which marks out the reference transit pattern for materials which do not leave the hepatic sinusoid; ^{22}Na, as a reference extracellular cation, which freely enters the interstitial space of the liver and marks out that part of the lobular extracellular space immediately available to cations of that size, but which is not significantly taken up by the liver cells during the time of a single passage (7); and ^{86}Rb, the substance under study, which we know undergoes relatively rapid concentrative uptake by the liver cells.

Friedman has suggested that dog red cells take up about 4.5% of plasma ^{86}Rb radioactivity almost immediately (9). In order to assess whether in vivo red cell carriage of the ^{86}Rb significantly modifies the form of the outflow curve for the ^{86}Rb, two varieties of experiments were carried out (10). In the first, the injection mixture consisted of ^{51}Cr-labeled red cells, and of plasma to which had been added ^{22}Na and ^{86}Rb. The hematocrit of this mixture was adjusted to match that of the peripheral blood and the mixture was constituted more than 2 min before the experiment. This material was placed in a single syringe for injection. In the second, the hematocrit of the animal was reduced by bleeding and dextran infusion and two injection mixtures were constituted: a first consisting of ^{51}Cr-labeled red cells suspended in plasma, with a hematocrit twice that of peripheral blood; and a second, consisting only of plasma to which had been added ^{86}Rb and ^{22}Na. These mixtures were placed in two separate syringes and an injection block was used which had been designed to provide continuous equal mixing of the materials of the two syringes at the point of injection. The hematocrit of the injected material thus matched that of the animal but the red cells were not exposed to the ^{86}Rb-containing plasma for a significant period of time prior to the experiment. Without prior bleeding of the animal, the hematocrit in the syringe containing red cells would have been so high that rapid injection in the absence of significant hemolysis would not have been possible. In each of the varieties of experiment, the materials were injected into the portal vein as rapidly as possible and serial effluent hepatic venous blood samples were collected over the next 30–60 s.

Special materials. The following special materials were used: [$^{51}Cr_2$]Na_2O_7 solution, 6 Ci/mmol;[1] [^{22}Na]Cl, 5 mCi/mmol;[2] and [^{86}Rb]Cl, 50 μCi/mmol.[3] The quantities of radioactivity injected for each experiment were approximately: ^{51}Cr-labeled red cells, 20 μCi; ^{22}Na, 3 μCi; and ^{86}Rb, 150 μCi.

Operative procedure and collection of samples. The experiments were carried out on mongrel dogs weighing 13–26 kg, which had been anesthetized with pentobarbital, 25 mg/kg. A catheter for injection was placed in the common portal vein (11) and a collection catheter, in the left hepatic venous reservoir (12), in such a fashion that no outflow obstruction was produced. The abdomen was closed for at least 30 min prior to the experiment, in order to allow the contents to return to a uniform temperature. The injection material was introduced rapidly, in order to produce turbulence and hence cross-sectional mixing, at the point of injection. With the hematocrits used, no hemolysis resulted. Hepatic venous samples, pumped from the outflow catheter with a Sigmamotor finger pump (Schaar Scientific Inc., Chicago, Ill.), were collected serially at a rate of about one per second. The collection catheter had a volume of 2.89 ml and the sampling rate varied around 65 ml/min.

Analysis of samples. Standards were prepared from each injection mixture by addition, in serial dilution, of blood obtained from the hepatic vein before collection of samples. ½ ml of sample or of diluted standard was pipetted into 1.0 ml of saline and centrifuged. The sample was assayed in a Nuclear-Chicago two-channel well-type scintillation crystal gamma-ray spectrometer (Nuclear-Chicago Corp., Des Plaines, Ill.) for gamma rays of appropriate energy (the areas of the gamma ray spectrum utilized were: the segment above 1.16 meV for ^{22}Na; the 1.08 meV area, for the photopeak of ^{86}Rb; and the 0.32 meV area, for the photopeak of ^{51}Cr). The upper and middle, the middle and lower channels were surveyed sequentially. In the middle and lower channels where the emissions from two and three substances, respectively, were present in the same channel, the activity due to each species was determined by use of appropriate standards and a decay factor. Where samples contained low activity, at least 1,000 counts were recorded in the lowest activity channel.

RESULTS

A dilution pattern corresponding to each of the injected substances was detected in the hepatic venous blood. In

[1] Charles E. Frosst and Co., Montreal, Canada.
[2] The Radiochemical Centre, Amersham, England.
[3] New England Nuclear Corp., Boston, Mass.

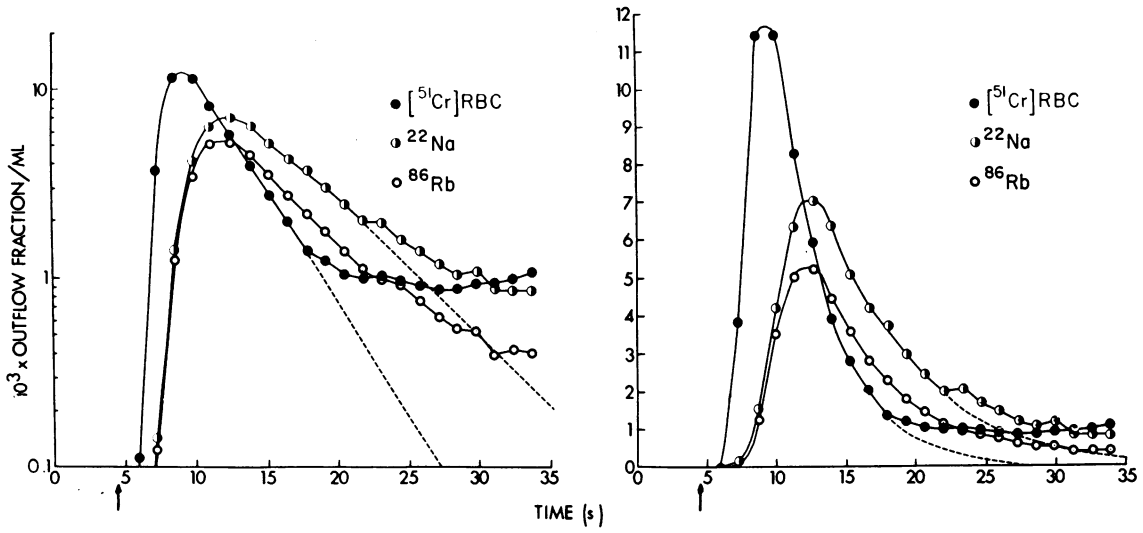

FIGURE 1 A typical set of dilution curves. This set was derived from a dual injection experiment. *Ordinates:* outflow fraction per milliliter. A logarithmic scale is used in the left hand panel and a linear scale, on the right. *Abscissas:* time in seconds. The arrow indicates the time delay of the input and collection systems. The values are plotted at mid-intervals.

order to produce a normalization of these patterns (and hence a basis for comparison within each experiment), the total injected amount of each material was defined as 1 unit, and the outflowing material was quantitated as a fraction of the injected amount per milliliter (i.e., a reciprocal volume). The kinds of curves resulting from each kind of experiment (that in which the labeled red cells were preincubated for more than 2 min, and that in which the double injection was used) were virtually identical. Fig. 1 illustrates a typical experiment. Detectable activity corresponding to labeled red cells, but not to the two other indicators, is evident in the first sample. The outflow fraction per milliliter for labeled red cells rises to the highest and earliest peak and decays rapidly until recirculation occurs. The values for labeled sodium are lower on the upslope; the peak for this curve is lower and is delayed so that it falls beyond the downslope of the labeled red cell curve; the downslope decays much more slowly; and recirculation appears later. The labeled rubidium curve is related to the labeled sodium curve in such a fashion that the first part of it appears to be "contained" within the labeled sodium curve. The values for rubidium on the upstroke of the curve are only slightly lower than those for the labeled sodium. On the semilogarithmic plot the rubidium curve thereafter progressivly diverges from the sodium curve. The peak of the rubidium curve is lower and slightly earlier; and the initial downslope decays more rapidly than does that of the labeled sodium curve. The slope of the rubidium curve then decreases substantially at the time when recirculation is evident on the sodium curve.

The downslopes of the labeled red cell and labeled sodium curves were extrapolated on semilogarithmic plots to yield primary dilution curves, as suggested by Hamilton, Moore, Kinsman, and Spurling (13). The areas under the primary labeled red cell and labeled sodium curves are equivalent. For these experiments the ratio of the area under the labeled sodium curve to the area under the labeled red cell curve was 0.997±0.062 (SD). The two values therefore yield equivalent values for flow, and indicate that the first passage recovery of labeled sodium is complete. We would expect that the ^{86}Rb which enters liver cells would be exchangeable and that the area under a complete first passage rubidium dilution curve would be equivalent to that for the two reference substances (14). If we apply the extrapolation procedure to the rubidium curve we define a component re-

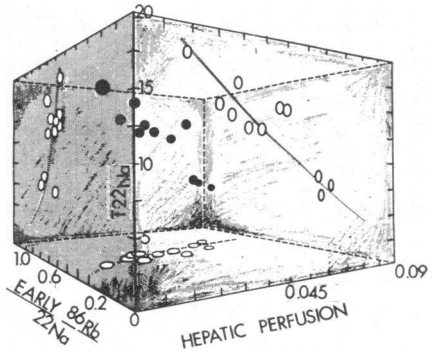

FIGURE 2 Relation between hepatic perfusion, transit time for ^{22}Na, and the relative "early" rubidium recovery.

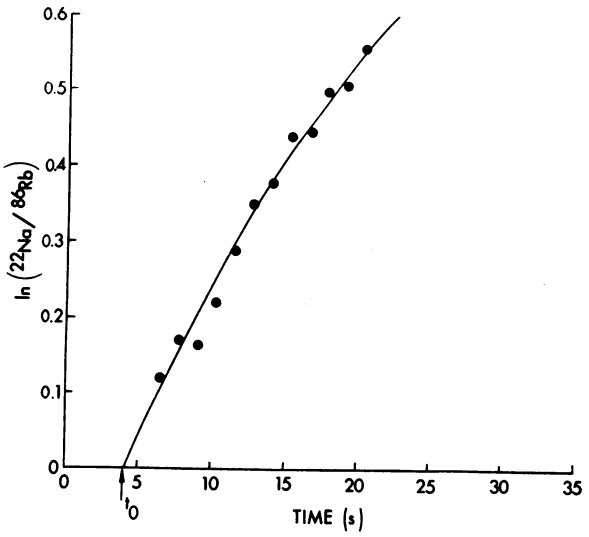

FIGURE 3 Natural logarithm of the ratio ([^{22}Na outflow fraction per ml]/[^{86}Rb outflow fraction per ml]) vs. time. The values are plotted at mid-intervals.

lated in time to the labeled sodium curve, but reduced in area. We fail to recover the whole of the primary dilution curve, although we have defined an apparent early component of this curve. The later part of the curve is not separable from recirculating label, by inspection, and the lack of ease of separation leads to the inference that it is a prolonged low-in-magnitude tailing. In Fig. 2 we have illustrated the relation between the hepatic perfusion (blood flow per unit tissue weight in $ml \cdot s^{-1} \cdot g^{-1}$), ^{22}Na transit time (seconds), and the extrapolated relative "early" rubidium recovery. The range of values for hepatic perfusion, produced by deliberate bleeding and dextran and saline replacement, is wide. The trends to be noted are the decrease in ^{22}Na transit time with increasing perfusion, and the concomitant decrease in the apparent early extraction of ^{86}Rb. The average early recovery of ^{86}Rb, in relation to that for labeled sodium, was 0.64. These values and other parameters obtained directly from the data are assembled in Table I. The mean transit times were obtained from the extrapolated curves (that for rubidium refers only to the extrapolated early component), and were corrected for input and output delays by subtraction of the appropriate times.

No further insight of consequence can be obtained without the use of modeling. With it, descriptive parameters and quantitative predictions otherwise inaccessible may be obtained. We therefore develop, in an Appendix, a kinetic model to describe the uptake process for rubidium. This modeling, in essence, consists of a delayed wave flow-limited distribution of plasma label out to the cell surface, with concomitant concentrative transport into the cell. The modeling is distributed in space and the temporal relations between the observed outflow fractions per milliliter for the three substances (vascular reference, extracellular reference, and rubidium) are viewed as consequent to events occurring upstream from the point of observation.

The characteristics of the modeling are best understood by reference to Fig. 9, in the Appendix. The outflow profile for the substance entering cells consists of two parts: throughput material, which propagates along in the sinusoid and extracellular space without entering the cell; and returning material which has entered the cells and later returned to the plasma space. As the transport process becomes progressively more concentrative, the returning material becomes progressively reduced in magnitude and prolonged in time. Hence,

TABLE I

Transit Time and Flow Data from the Dilution Curves

Exp. no.	Body wt	Liver wt	Hematocrit	Hepatic perfusion	$\bar{t}_{RBC}$	$\bar{t}_{Na}$	$\bar{t}_{Rb}$ early	Early Rb/Na
	kg	*g*		$ml \cdot s^{-1} \cdot g^{-1}$	*s*	*s*	*s*	
1	16	540	0.44	0.014	8.26	17.85	16.20	0.55
2	15	558	0.25	0.056	4.52	8.76	8.16	0.73
3	14	326	0.42	0.044	7.24	14.47	13.54	0.64
4	15	352	0.40	0.043	7.05	14.51	13.04	0.56
Dual injection experiments								
5	14	455	0.17	0.031	8.81	13.41	12.72	0.68
6	27	891	0.26	0.029	10.80	16.49	15.76	0.69
7	16	569	0.19	0.036	7.45	13.33	12.44	0.62
8	15	492	0.22	0.058	4.52	7.37	7.20	0.63
9	20	660	0.19	0.023	8.07	14.30	13.27	0.62
10	18	506	0.23	0.027	7.98	13.98	12.34	0.56
11	14	461	0.21	0.062	4.23	8.26	6.81	0.78

for the highly concentrative rubidium transport process we would expect the second component to be very prolonged and low in magnitude.

Use of modeling to analyze these dilution experiments. Four calculable natural parameters arise from the modeling. Their numerical values can be determined from the interrelations between the curves for the vascular reference, extracellular reference, and exchanging material. They are: $p\gamma$ (the extracellular space ratio, the product of the partition coefficient p for the substance in the extracellular space and γ, the ratio between the extracellular space and the accessible sinusoidal space), t_o (the large vessel transit time), $k_1\theta/[1 + p\gamma]$ (the cellular influx rate constant, multiplied by the ratio of the cellular space to the total space, vascular + extracellular, outside the cells), and k_2/r (the cellular efflux rate constant, divided by the partition coefficient for rubidium in the intracellular space). In our present experiments we will expect (both from the forms of the dilution curves and from the computed illustration of the single sinusoid modeling) that the ratio k_1/k_2 will be very large, and that the second component of the curve for the exchanging material will be a low-in-magnitude and very prolonged tailing. We assume in these experiments that p and r are unity.

We derive first estimates of $p\gamma$ and t_o by use of the graphical maneuvers which we have described previously (11). Then we have the task of obtaining a rough estimate of the parameter $k_1\theta/[1 + p\gamma]$. In our modeling we show that the early throughput material emerges at a time when the ^{86}Rb returning from the cells contributes no quantitatively important component to the outflow curves; and that the throughput material is quantitatively related to the extracellular reference by the damping factor $\exp[-(k_1\theta/[1 + p\gamma])(t - t_o)]$. Hence we have plotted the natural logarithm of the ratio of the sodium to rubidium outflow fractions per milliliter vs. time (Fig. 3) and have utilized the initial slope as our rough estimate of the parameter $k_1\theta/[1 + p\gamma]$. We would expect this plot to show a continuing rising linear relation if the returning ^{86}Rb contributed no important component to the outflow, later in time. We have previously observed such a relation between the outflow curves for labeled albumin and sulfobromophthalein (the latter is bound to albumin, transported into the liver cells in a concentrative fashion, and removed from the cells by biliary excretion). In this figure, however, the initial values scatter about a rising linear relationship and the later values are somewhat lower than the extrapolated linear relation, as would be expected if a small amount of the rubidium entering cells were returning to the circulation. The initial estimate of the parameter k_2/r was therefore taken to be a finite value, but one much smaller than that for $k_1\theta/(1 + p\gamma)$

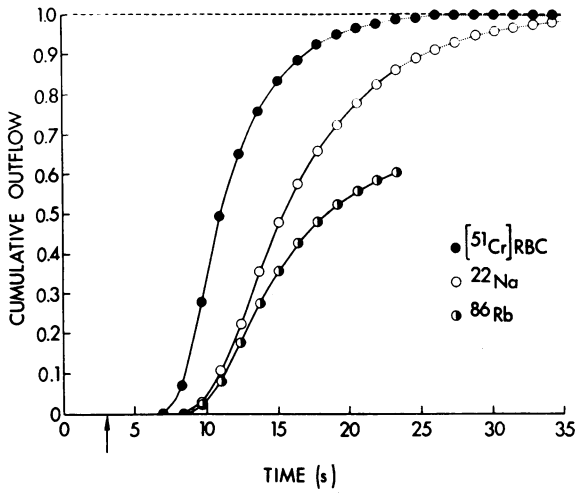

FIGURE 4 Cumulative outflow of each indicator vs. time. The dotted parts of the curves for labeled red cells and labeled sodium correspond to the linear extrapolations on the semilogarithmic panel of Fig. 1. The cumulative ^{86}Rb curve is represented only until that point in time where recirculation of the ^{22}Na has occurred. Representation beyond that point would necessarily be arbitrary extrapolation. The values are plotted at end-intervals.

All four of these parameters were then optimized on an IBM 360 model 65 digital computer, by use of a set of programs designed to minimize the sum of the squares of the differences between computed and observed values. We initally attempted to fit three arbitrarily defined functions to the labeled red cell dilution curves, a random walk (15), a lagged normal density distribution (16), and a gamma function (17), to serve as a first starting point. We were unable to fit the curves very precisely with any of these and so decided to use numerical interpolation to provide data points within the intervals when they were needed. In designing the interpolation procedure, we found that it was necessary to handle the data in the following manner. Each sample collected is mechanically integrated over the sampling period and hence it is treated mathematically as an integrated sample over that period. Therefore, although single interval values of the outflow fraction per milliliter should be plotted against midinterval times, as a histogram type of representation (we have instead joined these points in our illustrations), the cumulative outflow fraction per milliliter is precisely defined at end interval times and a continuous function may be generated through these points (see Fig. 4). This latter type of data was therefore used as the basis for interpolation.

The initial graphical estimates of $p\gamma$ and t_o were optimized by means of an iterative procedure in which the time scale of the ^{22}Na curve beyond t_o was diminished, and the magnitude of the curve increased by a single factor, so as to make it superimpose upon the red cell

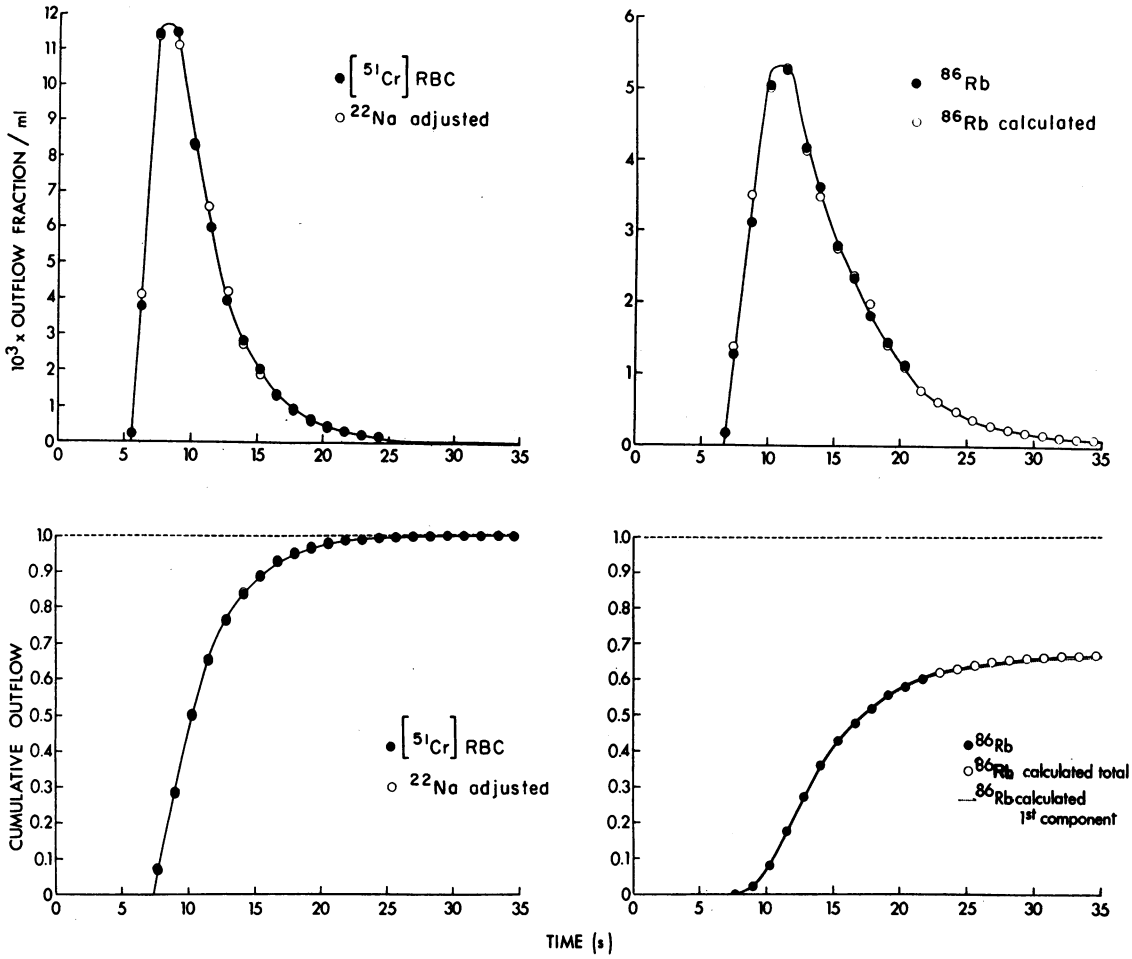

FIGURE 5 Illustration of the fitting procedures. The panels on the left illustrate the superimposition of the adjusted ^{22}Na curves upon the ^{51}Cr-labeled red cell curves. The panels on the right illustrate the concordance between the computed and experimental ^{86}Rb curves. For the cumulative curve the differences are so small that they cannot be illustrated. The extrapolation of the cumulative ^{86}Rb curve corresponding to the fitted rate constants and the calculated throughput component of this curve are displayed. The values for the upper panels are plotted at mid-intervals; those for the lower, at end-intervals.

curve (see Fig. 5; and equation 7 *C* of the Appendix). Small differences between the labeled red cell and adjusted ^{22}Na curve are evident, but are not easily visible when the cumulative representation is used. The average relative coefficient of variation for the fitting procedure (histogram type) was 0.070, for this group of experiments. A second iterative procedure was then used to generate from the ^{22}Na curve a computed ^{86}Rb curve which optimized the $k_1\theta/(1 + p\gamma)$ and k_2/r values in such a fashion as to provide the best possible fit to the experimental ^{86}Rb curve. The average relative coefficient of variation for this procedure was 0.080. The differences between computed and experimental curves are small, and on the cumulative illustration, are too small to present visually. The returning component (the difference between the throughput and total rubidium outflow, in Fig. 5) is exceedingly small in magnitude and its initial contribution to the cumulative outflow is exceedingly small. Since the cumulative outflow curve corresponds to the results of a steady infusion, we see that the material which would emerge at the outflow, early in the course of such an infusion, would be almost completely throughput material. Little of the material arriving at the outflow early in time will have entered cells.

The relation between the calculalted values for $k_1\theta/(1 + p\gamma)$ and the hepatic perfusion rate (flow per unit weight) is illustrated in Fig. 6. There is a modest scatter in the values but no overall trend is evident. The values appear to remain fairly constant over the range of perfusion rates which occurred in this set of experi-

ments. The average value for this parameter was 0.043± 0.007 (SD) s^{-1}. Since this parameter defines the proportion of the Rb^+ which emerges as throughput it is apparent that the increase in throughput with increase in perfusion, illustrated in Fig. 2, and the corresponding decrease in the apparent relative "early" extraction of Rb^+ with increase in perfusion, has resulted predominantly from a change in the exposure time during passage along the sinusoid. The parameter $k_1\theta/(1+p\gamma)$ may also be shown to be equal to $k_1'\varphi L/(A+pB)L$, i.e. the product of the cellular influx transport rate coefficient per unit area k_1' and the ratio between the active cell surface facing the sinusoid φL and the total sinusoidal and extracellular volume of distribution available to rubidium $[A+pB]L$. One would not expect the transport rate coefficient per unit area k_1' to change with flow, unless flow became so low that the supply of energy by oxidative metabolism became impaired. The lack of change in the parameter $k_1\theta/(1+p\gamma)$ with flow may therefore be interpreted to mean that the ratio $\varphi L/(A+pB)L$, i.e., the ratio between the active cell surface facing the sinusoid and the total extracellular space of distribution available to Rb^+, has not changed with flow. In this series of experiments the ^{22}Na extravascular space (the analogue of BL, defined as the product of the plasma flow and the difference between the mean transit times of ^{22}Na and the ^{51}Cr-labeled red cells), when expressed as a proportion of liver weight, showed a small increase with perfusion. This change, when coupled with the preceding observations, leads to the suggestion that there was perhaps also a small increase with perfusion in the number of pathways in which there was flow, over the range explored, but that in each the ratio $\varphi L/(A+pB)L$ remained constant. Although the estimate of the extravascular ^{22}Na space appears accurate, no secure way of estimating sinusoidal plasma volume, the analogue of

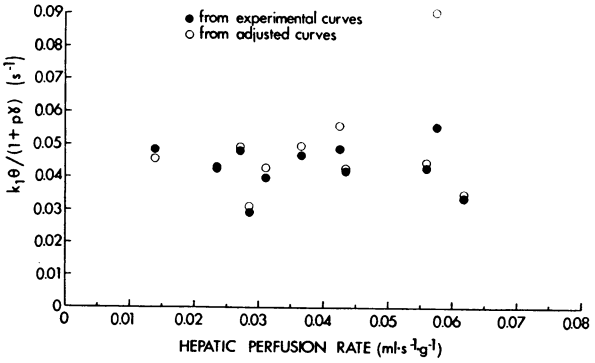

FIGURE 6 The relation between the calculated values for $k_1\theta/(1+p\gamma)$ and the hepatic perfusion rate. The filled circles represent values obtained from the experimental curves; and the empty circles, values obtained from the adjusted curves.

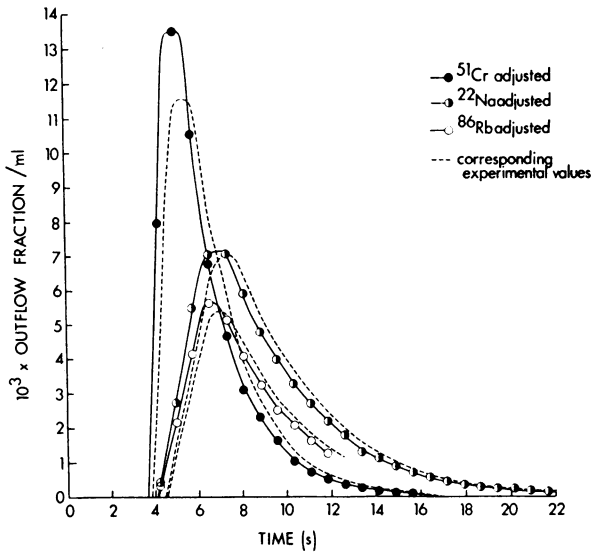

FIGURE 7 The adjusted and experimental dilution curves. The dashed curves are those illustrated in Fig. 1. The solid curves are the resynthesized curves. The points on the curves represent integrated values for each interval. In order to display the relation between the observed and undistorted curves, the time scales have been related in the following way: the time of injection for the dashed curves is zero; and that for the undistorted curves is the dead time of the collecting system, 1.86 s.

AL, has been found (the value provided by the t_0 value is too large [18]), and so a precise estimate of the total volume available for rubidium outside the cells, $(A+pB)L$, cannot be obtained. Thus a value for the product of k_1' and the active cell surface per unit liver weight, the analogue of a permeability surface product PS per unit tissue weight, cannot be secured. Despite our inability to calculate this parameter it is evident that it changes little with perfusion, over the range explored. In addition, no evident correlation was found between the rate constant $k_1\theta/(1+p\gamma)$ and the serum potassium level.

The ratio $k_1\theta r/k_2(1+p\gamma)$ may similarly be shown to be $(k_1'/k_2')\cdot(CL)/(A+pB)L$. For the whole liver this corresponds to (k_1'/k_2') times the ratio of the total cellular volume to the total available sinusoidal and extracellular volume. The average value for $k_1\theta r/k_2(1+p\gamma)$ in this group of experiments was 27.1±8.0 (SD).

Effect of the collecting system. The parameters obtained so far have come from the raw experimental data. However, the data have been altered by the collecting system. The response of this collecting system to a step input is a delay succeeded by a rising exponential (18). When the delay and distortion are removed from the data, by use of a process of deconvolution, the resynthesized curves, those which we would have observed in the absence of the collecting system, are found to rise more

steeply, peak earlier, and decay faster, the change being proportionately larger for those curves in which the rate of change in the outflow fraction per milliliter is largest (see Fig. 7). When the procedures outlined above are applied to these adjusted curves, the values for $p\gamma$ and t_0 increase, as expected (18); and the values for $k_1\theta/(1 + p\gamma)$ also increase to an average value of 0.048±0.014 (SD), a fractional increase of 0.12. The last parameter increased unduly in one experiment, but the number of data points on the dilution curves in that experiment was smaller and it appears that the adjustment procedure may well have been in error. For the whole group of experiments the value for the ratio $k_1\theta r/k_2(1 + p\gamma)$ changed little. The new average value was 25.9±7.4 (SD). Thus, proportionately, the effect of the collecting system on the numerical estimates of the parameters dealing with transport has not been great. We may therefore, by analogy, conclude that the distorting effect of the large veins in the liver (which remains in the adjusted curves) is not so large as to invalidate the major conclusions arising in this study.

DISCUSSION

Form of the experimental data. The data indicate that after a single injection approximately 40% of labeled rubidium is taken up by the liver; and may be inferred to mean that, early in time, following a steady trace infusion, the same proportion would be removed.

Characteristics and utility of the modeling developed here. In the liver the entrances and exits to the sinusoids are adjacent and the flow in the adjoining sinusoids is concurrent. The effect of diffusional interconnection between the sinusoids (19) may therefore be expected to be minimal. Within this framework we have developed the simplest possible kind of model, one in which longitudinal transport occurs only by flow (i.e., in which axial diffusion, in the direction of flow, is neglected [20]). The numerical analysis carried out by Bassingthwaighte, Knopp, and Hazelrig (in which a variety of flow rates and Krogh cylinder sizes were explored) make this assumption relatively reasonable (21). We have then superimposed upon this the transport phenomena at the cell surface adjacent to the space of Disse, and have described two components to the outflow from a sinusoid following a rapid injection, throughput and returning material, and have shown that, when the transport process is highly concentrative, the throughput material may be expected to emerge relatively uncontaminated by returning material. The uptake process for rubidium is highly concentrative and so the concentrative extreme of the modeling was fitted to the data. Within the rubidium data the material returning from the cells later in time is largely obscured by recirculation and so the part of the modeling dominating the fitting procedure for obtaining transport parameters from these data was necessarily that relating to the throughput material.

The major problem encountered was that of determining the distribution of hepatic sinusoidal transit times. The experimental examination of a concentrative transport case has permitted us to gain some insight into this. In other organs, authors have assumed that there is a single uniform transit time through the exchange area, the capillary bed (19–23); and some have used a single part of the curve (22, 23), either upslope or peak, for the calculation of the transport parameters. It has been our purpose here to utilize the whole of the reliable experimental information (upslope, peak, and early downslope) to calculate parameters. If we consider the whole curve then we find that, if there had been a single sinusoidal transit time, the rubidium throughput component would have been a scaled replica of the labeled sodium curve. It clearly is not, even on inspection, and so we rejected this possibility. We then examined the remaining possibilities, that there is a distribution of large vessel and sinusoidal transit times and the other extreme, that the large vessel transit times are uniform. Preliminary attempts at computing, where arbitrary distributions of large vessel and sinusoidal transit times were used, indicated that the last possibility was close to correct and so we chose this. This simplification has another major advantage. As a direct consequence of it, we arrive at a small enough number of variables that use of the data to arrive at single values of the parameters becomes possible. A second consequence of this assumption is less good, in this particular instance. Since only the very early part of the ^{86}Rb returning from the cells has been accessible in the reliable part of the experimental data (that part returning prior to recirculation of the ^{22}Na label), i.e., since a major part of the accumulated tail functions is missing from the data, the procedure used to fit the modeling to the data to gain an estimate of k_2/r cannot be expected to yield a very precise estimate. The order of magnitude of the estimate appears correct, but no great reliance can be placed upon its numerical accuracy.

In the present experiments we have assumed that the values of k_1 and k_2 at the liver cell membrane are linear with changes in concentration. Since the concentration of Rb^+ used was exceedingly low, the assumption appears reasonable. The effect of changing the concentration of Rb^+ upon the values of the rate constants was not explored, because of the potential of high Rb^+ concentrations for producing undesirable cardiac side effects.

The response to constant infusion. The present description of the single passage uptake of Rb^+ provides a bridge for the understanding of the more classical method for examining the uptake of substances like this,

that of constant infusion. Our analysis indicates that the throughput component contributes to the initial plateau and that the slow decrease in extraction with time which ensues is the result of a gradually increasing return to the circulation of Rb^+ which has entered cells. Similar phenomena have been observed in skeletal muscle and they will be expected to have a qualitatively similar explanation (22). The major expected areas of difference in the description of phenomena in skeletal muscle will be in the degree of heterogeneity in the preparation, the distribution of small and large vessel transit times, and the presence of a poorly permeable passive capillary barrier between the vessel lumen and the active cell surface.

It is of interest to pursue somewhat further the analogy between the present formulation and that used by Renkin (22) and by Crone (23). From equation 5 E in the Appendix, we find that the throughput term of the sinusoidal response to a steady infusion is $(q_0/F_s)\exp(-k_1S_s/F_s)S(t-[1+p\gamma]\tau)$, where $S(t-[1+p\gamma]\tau)$ is a step function emerging at $t=[1+p\gamma]\tau$. If one then assumes, as the above authors did, that the sinusoidal transit time is the same for each element of vascular fluid passing through the organ, the damping term in this expression is common for each part of the effluent fluid; and, if the mechanism at the barrier is grossly concentrative, or if the material beyond the barrier is effectively removed (e.g. by the muscle cell surface beyond the capillary, in skeletal muscle), the cumulative throughput will define an early plateau value, which may be used to calculate the approximate value of the parameter $k_1'S_s/F_s$. For a capillary the value for γ is zero, and the damping term becomes $\exp(-PS_c/F_c)$, where P is the permeability of the capillary, S_c is its surface area, and F_c is the flow through it. In contrast, in the situation which we have examined in the present paper, the sinusoidal transit times appear to be distributed, to have many values, and therefore a distribution of values for the ratio (S_s/F_s) results. Hence we have been able to derive no single corresponding value for $k_1'S_s/F_s$ from the data. A rather more complex constant, $k_1\theta/(1+p\gamma)$, equivalent to $k_1'\varphi/(A+pB)$, with the dimensions time^{-1}, has been defined.

Effect of the collecting system. The lack of major change in the values of the parameter $k_1\theta/(1+p\gamma)$ after the data have been adjusted for the distortion in the collecting system gives some confidence that these values are of the right order of magnitude, and that the remaining large vessel distortion has probably not produced a major change in the estimate.

Comparison between the removal of ^{86}Rb by the liver and by skeletal muscle. The "early" hepatic clearance of ^{86}Rb after trace infusion (the product of the hepatic perfusion and the apparent early single passage extraction) is much larger than that of skeletal muscle, at any given flow rate (see Fig. 8). The "early" plateau extraction of ^{86}Rb by isolated perfused resting skeletal muscle is 0.62 at a flow of 0.02 ml·min^{-1}·g^{-1}; and it drops to 0.20 at a flow of 0.08 ml·min^{-1}·g^{-1} (9). In contrast, corresponding values for the mean regression line fitted to our liver data are 0.43 at 1.0 ml·min^{-1}·g^{-1}; and 0.27 at 4.0 ml·min^{-1}·g^{-1}. Although the capacity of intact skeletal muscle for the transport of these essentially tracer doses of radioactive Rb^+ would be expected to be higher during exercise, it would be surprising if differences of this order of magnitude were abolished. It is not clear whether the relative limitation in the capacity of skeletal muscle to take up ^{86}Rb lies in the diffusion barrier at the capillary membrane; or in the capacity of the transport system situated at the muscle cell surface.

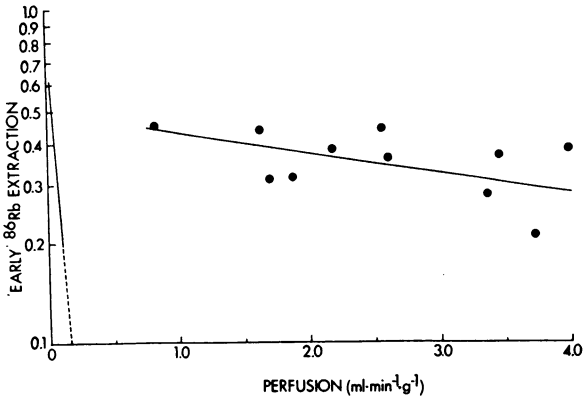

FIGURE 8 Contrast between the relation of extraction to perfusion, in the liver and in muscle. The data points are derived from the present experiments and the regression line fitting these data is ln (extraction) $= -0.154$ (perfusion) $- 0.689$. The correlation coefficient for this semilogarithmic plot is 0.63. The regression line fitted by Friedman (9) to his data on skeletal muscle, ln (extraction) $= -12.6$ (perfusion) $- 0.226$, is displayed on the left of the panel. The predicted clearance of ^{86}Rb by skeletal muscle would be expected to be an order of magnitude smaller, if the perfusion in skeletal muscle had been of the same order as the hepatic perfusion.

Further applications. This study and the modeling used to gain insight into it provide a background for further study. The two areas in which the techniques developed here will find immediate application are: the examination of the kinetic behavior of substances undergoing approximately equilibrative transport, which are not removed to any major extent within the cells, and which are therefore potentially completely recovered fairly quickly at the outflow following a single injection (e.g., for glucose, approximations to both transport rate coefficients should be accessible); and the examination of substances which are removed within the cells, so that the outflow recovery of the substance is incomplete. In the latter instance the extension of the modeling to

include effective removal from the intracellular tracer pool will lead to a relatively complete description of the kinetics of the distribution of both substances like labeled galactose, which is metabolically sequestrated within the liver, and substances like sulfobromophthalein and bilirubin, which undergo conjugation and subsequent removal by biliary excretion.

APPENDIX

The events in a single sinusoid. Consider a sinusoid of length L in which blood flows with the velocity W, which is enfolded by an extracellular space, the space of Disse. There is no permeability barrier between the sinusoids and the space of Disse, and the dimensions of the space and the times of exposure are such that diffusible substances in the plasma phase may be expected to reach essentially their equilibrium concentration in the space of Disse at each point along the length (11, 24). The cellular space enfolds the extracellular space and is separated from it by a cell membrane, a permeability barrier at which membrane transport phenomena may be expected to occur. The depth of the cellular space in the liver is such that lateral diffusion equilibration will also be expected to occur within the cells, during the time of exposure. Now let W = the velocity of flow in the sinusoid; $u(x,t)$ = the concentration in the sinusoid at some point along the length x, at the time t; $v(x,t)$ = the corresponding concentration in the adjacent extracellular space; $z(x,t)$ = the concentration in the cells; $A,B,C,$ = the volume per unit length for capillary, extracellular space, and cellular space, respectively (they are regarded as constant along the length); $B/A = \gamma$, and $C/A = \theta$; and p,r = the partition coefficients for the substance under consideration in the extracellular space and intracellular phase, with respect to the corresponding equilibrium plasma concentration, as suggested by Perl and Chinard (20). These parameters describe the relative solubilities of the substance in those phases.

If we assume that the mechanism for transport along the length is vascular flow (that lengthwise movement by diffusion can be neglected, within the time periods being considered) then it follows from mass continuity that the change in quantity of material in the system (including sinusoid, extracellular and cellular spaces) between any x and $x + \Delta x$ during any fixed interval of time Δt is exactly the change in quantity of material in the sinusoid alone between time t and $t + \Delta t$ over the volume element between x and $x + \Delta x$. The rate of change of material in the sinusoid per unit length between x and $x + \Delta x$ (the blood flow through the sinusoid multiplied by the gradient in concentration across the interval) is $-AW\frac{\partial u}{\partial x}$; and the rate of change of material in the whole volume element per unit length is $A\frac{\partial u}{\partial t} + B\frac{\partial v}{\partial t} + C\frac{\partial z}{\partial t}$. Whence, equating these, we find

$$\frac{\partial u}{\partial t} + W\frac{\partial u}{\partial x} + \gamma\frac{\partial v}{\partial t} + \theta\frac{\partial z}{\partial t} = 0. \qquad (1)$$

Now consider that the material under consideration is undergoing flow-limited distribution from the sinusoidal to the extracellular space. Then $v(x,t) = pu(x,t)$ and $\partial v/\partial t = p\partial u/\partial t$, and so

$$\frac{(1 + p\gamma)}{W}\frac{\partial u}{\partial t} + \frac{\partial u}{\partial x} + \frac{\theta}{W}\frac{\partial z}{\partial t} = 0. \qquad (1A)$$

Now we must formulate an equation describing the transport of material from the extracellular space to the cellular interiors. The process of transport may of itself produce an increase or a decrease in the concentration of material across the cellular membrane at equilibrium, i.e., there may be an asymmetry in the concentration dependence of influx and efflux and so two rate constants will be used. The rate of cellular influx of material is assumed proportional to the product of the cell surface per unit length ϕ, the length under consideration Δx, the rate constant for uptake per unit area k_1' (with dimensions $cm \cdot s^{-1}$ [25]), and the product of p^{-1} and the extracellular concentration $v(x,t)$; and the rate of efflux to the extracellular space, proportional to the product of $\phi \cdot \Delta x$, the rate constant for exit per unit area k_2' (dimensions $cm \cdot s^{-1}$), and the product of r^{-1} and the cellular concentration $z(x,t)$. Hence,

$$\frac{\partial z}{\partial t} = \frac{k_1'\phi}{C}\frac{v}{p} - \frac{k_2'\phi}{C}\frac{z}{r}$$

$$= k_1 u - k_2\frac{z}{r}, \qquad (2)$$

where $k_1 = k_1'\phi/C$; and $k_2 = k_2'\phi/C$. When the transport system is an equilibrative one $k_1' = k_2'$; and when it is concentrative $k_1' > k_2'$. Eliminating z from these equations we find

$$\frac{\partial^2 u}{\partial t^2} + \left(\frac{W}{1 + p\gamma}\right)\frac{\partial^2 u}{\partial x \partial t} + \left[\frac{k_1\theta}{1 + p\gamma} + \frac{k_2}{r}\right]\frac{\partial u}{\partial t}$$

$$+ \frac{k_2}{r}\frac{W}{(1 + p\gamma)}\frac{\partial u}{\partial x} = 0. \qquad (3)$$

Solution of the equations for a single sinusoid. Now introduce into the initially empty sinusoid of length L with flow F_s a quantity of diffusible material q_0 at the time $t = \epsilon$ (a value infinitesimally greater than zero), at $x = 0$. Equation 3 must then be solved according to the initial conditions

$$u(0,t) = \frac{q_0}{F_s}\delta(t - \epsilon); \quad \text{and}$$

$$u(x,0) = 0, z(x,0) = 0, \quad \text{and} \quad u'(x,0) = 0, \qquad (4)$$

where $\delta(t - \epsilon)$ is an impulse or Dirac delta function.

Now if to equation 3 we apply the Laplace operator with respect to time,

$$\mathfrak{L}(f[x,t]) = \int_0^\infty f(x,t)e^{-st}dt = \bar{F}(x,s)$$

we find

$$\bar{U}(x,s) = \bar{U}(0,s)$$

$$\times \exp\left[-\frac{sx}{W}(1 + p\gamma)\left(1 + \frac{k_1\theta/[1 + p\gamma]}{s + [k_2/r]}\right)\right],$$

whence (15)

$$u(x,t) = \frac{q_0}{F_s}\exp\left(-\frac{k_1\theta t}{1+p\gamma}\right)\delta\left(t-[1+p\gamma]\frac{x}{W}\right) + \frac{q_0}{F_s}\exp\left(-k_1\theta\frac{x}{W}\right) \times\sum_{n=1}^{\infty}\frac{\left(k_1\theta\frac{k_2}{r}\frac{x}{W}\right)^n\left(t-[1+p\gamma]\frac{x}{W}\right)^{n-1}\exp\left[-\frac{k_2}{r}\left(t-[1+p\gamma]\frac{x}{W}\right)\right]}{n!(n-1)!}S\left(t-[1+p\gamma]\frac{x}{W}\right), \quad (5)$$

where $S\left(t-[1+p\gamma]\frac{x}{W}\right)$ is a step function at $t=(1+p\gamma)\frac{x}{W}$.

In order to gain insight into our modeling, we will consider the outflow response from the sinusoid of length L, in the following cases:

I. $k_1 = k_2 = 0$; and $\gamma = 0$. In this case, which corresponds to the labeled red cells, the vascular reference substance,

$$u(L,t) = \frac{q_0}{F_s}\delta\left(t-\frac{L}{W}\right). \quad (5A)$$

A labeled red cell will be carried along the sinusoid with the velocity of flow and emerge at the time $\tau = L/W$.

II. $k_1 = k_2 = 0$; and γ finite. For our purposes the substance considered to exhibit this behavior is labeled sodium. Its outflow response is

$$u(L,t) = \frac{q_0}{F_s}\delta(t-[1+p\gamma]\tau). \quad (5B)$$

The labeled sodium undergoes flow-limited distribution into the extracellular space and consequently propagates along the capillary with the slower velocity $W/(1+p\gamma)$. It emerges delayed with reference to the red cells, at the time $(1+p\gamma)\tau$. The underlying assumption utilized here is that there will be no significant dispersion of the sodium bolus due to intravascular mixing processes. Since the flow pattern in the sinusoids is bolus flow (26) and since the displacement observed between the outflow patterns for labeled red cells and labeled albumin is not major in organs such as the lungs, where the latter tracer does not leave the capillaries significantly in a single passage (27), this assumption appears relatively reasonable. It will not be completely precise, however, and an intravascular mixing process will probably contribute a small amount of dispersion to the sodium curve. Despite this, it will continue to be an accurate indicator for what the outflow for labeled rubidium would have been, if none of the material had entered liver cells, and if the red cell uptake of rubidium can be neglected.

III. k_1, k_2, and γ finite. This outflow response, that of a substance entering and leaving liver cells, is

$$u(L,t) = \frac{q_0}{F_s}\exp(-k_1\theta\tau)\delta(t-[1+p\gamma]\tau) + \frac{q_0}{F_s} \times\exp\left[-\left(k_1\theta-\frac{k_2}{r}[1+p\gamma]\right)\tau\right]\exp\left(-\frac{k_2 t}{r}\right) \sum_{n=1}^{\infty}\frac{\left(k_1\theta\frac{k_2}{r}\tau\right)^n(t-[1+p\gamma]\tau)^{n-1}}{n!(n-1)!} \times S(t-[1+p\gamma]\tau) \quad (5C)$$

$$= \frac{q_0}{F_s}\exp(-k_1\theta\tau)\delta(t-[1+p\gamma]\tau) + \frac{q_0}{F_s}\exp\left[-\left(k_1\theta-\frac{k_2}{r}[1+p\gamma]\right)\tau\right] \times\exp\left(-\frac{k_2 t}{r}\right)\sqrt{\frac{k_1\theta\frac{k_2}{r}\tau}{t-[1+p\gamma]\tau}} \times I_1\left(2\sqrt{k_1\theta\frac{k_2}{r}\tau(t-[1+p\gamma]\tau)}\right) \times S(t-[1+p\gamma]\tau), \quad (5D)$$

where $I_1(z)$ is a first order modified Bessel function with argument z. None of the material emerges at the outflow until the time $t=(1+p\gamma)\tau$.

The outflow profile consists of two parts. The first is an impulse function emerging at the time $(1+p\gamma)\tau$ and damped by the term $\exp(-k_1\theta\tau)$. It is delayed by the time $p\gamma\tau$ in relation to the vascular reference substance, and the total material emerging in it is reduced from q_0 to $q_0\exp(-k_1\theta t/[1+p\gamma])$. This term represents throughput material, material which has traveled both in the sinusoidal and extracellular space, which has not entered the cells but has swept past their surface. The second part of the profile represents returning material, material which has entered the cells and which later has returned to the extracellular space and sinusoid.

Some insight into the physical aspects of the processes taking place can be gained by substituting the equivalent expressions for the rate constants (i.e., $k_1 = k_1'\phi/C$; and $k_2 = k_2'\phi/C$). If $\phi L = S_s$, the surface of the liver cells surrounding the sinusoid and subserving the transport process, $CL = V_{cl}$, the volume of the cells corresponding to that sinusoid, $AL = V_s$, the volume of the sinusoid, and $\tau = V_s/F_s$, we find that

$$u(L,t) = \frac{q_0}{F_s} \times\exp\left(-\frac{k_1'S_s}{F_s}\right)\delta(t-[1+p\gamma]\tau) + \frac{q_0}{F_s} \times\exp\left(-\frac{k_1'S_s}{F_s}\right)\exp\left[-\frac{k_2'S_s}{rV_{cl}}(t-[1+p\gamma]\tau)\right] \times\sum_{n=1}^{\infty}\frac{\left(\frac{k_1'S_s}{F_s}\cdot\frac{k_2'S_s}{rV_{cl}}\cdot\tau\right)^n(t-[1+p\gamma]\tau)^{n-1}}{n!(n-1)!} \times S(t-[1+p\gamma]\tau). \quad (5E)$$

The first component once again represents throughput material. The damping factor in the first term, $\exp(-k_1'S_s/F_s)$, is absolutely independent of the size of the cellular space. It is analogous to that developed by Renkin (22) and Crone (23), $\exp(-PS_c/F_c)$, to quantitate the outflow emergence of throughput material from a permeable capillary (where P is the permeability of the capillary in centimeters per second, S_c is the surface area of the capillary in square centimeters, and F_c is the flow through the capillary in cubic centimeters per second.

One aspect of the second component, the returning material, deserves attention. When there is a high concentration of a binding substance with large affinity for the exchanging material present inside the cells (28), the partition coefficient r will be greater than one, and this will concentrate the exchanging material in the cells by a mechanism apart from that situated in the cell membrane. The second component will consequently become lower in magnitude and more prolonged. The partition coefficient r will also increase when the exchanging material in plasma is bound to albumin and the concentration of that protein is diminished. Unlike some other substances, rubidium appears to be osmotically free in the cells and so, for this cation, r is probably one.

We previously modeled the single passage uptake of sulfobromophthalein from a hepatic sinusoid (25). At that time we used two assumptions: that the uptake was proportional to the amount of material present in the extravascular space; and that none of the material which entered cells returned to the sinusoid during a single passage, i.e., that the parameter $k_2 = 0$, and hence that the second component, the exchanging material in our present development, was zero. We have reexamined these assumptions and it now appears to us that it is more appropriate to consider, as we have here, that the cellular uptake rate is proportional to the concentration of material present at the uptake surface; and that a complete description of the uptake process must necessarily include a description both of the return from the cellular space and of the changes in concentration of material in the cellular space, as a function of time and position.

IV. k_1 and k_2 approach infinity. Then

$$u(L,t) = \frac{q_0}{F_c}\delta\left(t - \left[1 + p\gamma + \frac{k_1}{k_2}r\theta\right]\tau\right). \qquad (5F)$$

This asymptotic case has no application in the present study but it does provide direct insight into the manner in which the partition coefficients, space sizes, and rate constants would be expected to interact to affect the propagation of a substance undergoing flow-limited distribution into both the extracellular and cellular spaces.

Recoveries and mean transit times. If equation 5C is correct, the total amount of material emerging at the outflow $F_s\int_0^\infty u(L,t)dt$, should be q_0, the amount introduced into the system. If we integrate the two parts, throughput and exchanging material, we find the total associated with the first is $q_0\exp(-k_1\theta\tau)$; and that with the second, $q_0(1 - \exp(-k_1\theta\tau))$. We have also integrated the appropriate expressions for the mean capillary transit times, and find these to be τ for the vascular reference substance (by definition); $(1 + p\gamma)\tau$ for the extracellular reference substance; and $\left(1 + p\gamma + \frac{k_1}{k_2}r\theta\right)\tau$, for the exchanging substance.

Changes in the outflow profile from a single sinusoid, with changes in the initial rate of cellular entry, and of the steady-state concentration ratio. The outflow profile for a substance which enters and leaves hepatic cells from the extracellular space consists of throughput material followed by what we shall call the tail function, a function which is spread out in time, and which represents material which has entered and then left the hepatic cells (the second term of equation 5C). The partition of outflowing material between the two parts varies with k_1, and the shape of the computed tail function changes remarkably with changes both in the uptake rate constant k_1 and in the ratio k_1/k_2. In order to provide insight into this phenomenon, we have computed a set of numerical illustrations (Fig. 9) for the case in which $\gamma = 1.0$, $\theta = 10.0$, $\tau = 1.0$, $q_0 = 1$, and the partition coefficients p and r are unity. The abscissa is normalized to t/τ; and the ordinate, correspondingly, to $F_s\tau u(L,t)/q_0$. The upper panel shows the outflow emergence of the vascular reference substance, an impulse function of unit area, at 1.0 time unit; and the second panel, the emergence of our extracellular reference substance, an impulse function of unit area, at 2.0 time units. The third, fourth, and fifth panels illustrate the profiles for varying values of the uptake constant k_1. In each instance this parameter defines the proportion of the material which emerges with the initial damped impulse function. This initial spike is followed by the tail function and, in each instance, the tail functions corresponding to three k_1/k_2 ratios: 1.0, 3.0, and 5.0, have been displayed. The magnitude of the tail function is lower, early in time, for higher k_1/k_2 values and, because the mean transit time for the outflow profile increases with increase in this ratio, it finally becomes greater in magnitude at long times. When the value of k_1 is small ($k_1 = 0.003$) the tail function is a small in magnitude, low slope, exponential. When the value of k_1 increases, less of the area is associated with the initial spike and the tail functions become reshaped into functions which rise to a higher value and then diminish. When the value of k_1 becomes larger still, none of the area is associated with the initial spike, at the time $(1 + p\gamma)\tau$. All of it is associated with the tail function and there is an additional outflow delay in appearance, beyond the time at which the extracellular reference substance appears. With further increase in k_1 the tail functions become compacted in time until finally, in the flow-limited extreme ($k_1 \to \infty$), illustrated in the lowest panel, an impulse function of unit area emerges at the mean transit time defined by the value of the ratio k_1/k_2 for the exchanging substance.

Outflow profile from a single sinusoid in response to a step input. The outflow profile from a single sinusoid in response to a step input embodies the response to a steady infusion, i.e., it is the integral of the outflow response to a single injection (equation 5C) and consistst of the sum of a step function of magnitude $\exp(-k_1\theta\tau)$ at the time $(1 + p\gamma)\tau$ and of the time integral of the tail function. When k_1/k_2 is a relatively large number and when k_1 is relatively small, the outflow will appear to the experimentalist to consist only of the step function of magnitude $\exp(-k_1\theta\tau)$. In this situation there would then appear to be, relatively early in time, a net extraction of the exchanging material $E = 1 - \exp(-k_1\theta\tau)$.

Form of the concentration profile within the sinusoidal and extracellular space, and within the hepatic cells. The concentration profile within the sinusoid and extracellular space between input and output is described by equation 5. It is appropriate to examine the adjacent profile in the cells and to compare the two profiles. We find, from equation 2, that

$$\bar{Z}(x,t) = \frac{k_1\bar{U}(x,s)}{\left(s + \frac{k_2}{r}\right)},$$

whence

$$z(x,t) = k_1\frac{q_0}{F_s} \times\exp\left[-\left(k_1\theta - \frac{k_2}{r}[1 + p\gamma]\right)\frac{x}{W}\right]\exp\left(-\frac{k_2}{r}\right) \times \sum_{n=0}^{\infty}\frac{\left(k_1\theta\frac{k_2}{r}\frac{x}{W}\right)^n\left(t - [1 + p\gamma]\frac{x}{W}\right)^n}{n!n!} \times S\left(t - [1 + p\gamma]\frac{x}{W}\right) \quad (6)$$

$$= k_1\frac{q_0}{F_s}\exp\left[-\left(k_1\theta - \frac{k_2}{r}[1 + p\gamma]\right)\frac{x}{W}\right] \times\exp\left(-\frac{k_2}{r}t\right)I_0\left[2\sqrt{k_1\theta\frac{k_2}{r}\frac{x}{W}\left(t - [1 + p\gamma]\frac{x}{W}\right)}\right] \times S\left(t - [1 + p\gamma]\frac{x}{W}\right). \quad (6A)$$

The relation between the two profiles is again difficult to perceive. In order to illustrate how they are related, and how they change as a function of time, we have computed a set of illustrative numerical examples (see Fig. 10). We have once again utilized these values of the parameters: $\gamma = 1.0$, $\theta = 10.0$, $\tau = 1.0$, $q_0 = 1.0$, and p and r are unity. Changes in the length profiles are indicated at normalized time intervals of 0.4, and a value for k_1, 0.03, has been chosen which corresponds qualitatively to that which we expect experimentally for ^{86}Rb (it is of a magnitude such that a major proportion of the material injected emerges with the initial impulse function as throughput material). The material which has entered the cells and then returned emerges at the outflow as the tail function and we would expect the form and magnitude of the intravascular profile contributing to this to vary with the relative magnitude of k_2, i.e., with the ratio k_1/k_2. For the purpose of this illustration we have once again picked the same three values for this ratio: 1.0, 3.0, and 5.0. The first corresponds to the equilibrative case in which, at equilibrium, intracellular and extracellular concentrations of material would be expected to be equivalent; and the second and third, to the concentrative cases. For this particular set of numerical parameters the lengthwise concentration profile within the cells becomes relatively flat, once the initial wave has swept by and this distribution, in turn, leads to the slow washout previously illustrated. The value of k_1 is common to all three cases being considered and the value of θ is relatively large. The bulk of the trailing material is intracellular at the times being considered and the changes in cellular concentration which result with changes in the ratio k_1/k_2 are so little different that we have displayed them as a single common intracellular profile. When $k_1/k_2 = 1.0$ (i.e., when k_2 is largest) the intravascular profile is largest in magnitude; and with increase in the ratio, the magnitude of the profile decreases progressively. This decrease corresponds to our previous demonstration of a corresponding decrease in the magnitude of the outflow tail function early in time, with increase in the ratio k_1/k_2.

The long term response of the intracellular concentration to a steady input of material is worth noting. The final cellular concentration of material will be k_1r/k_2 times the input vascular concentration.

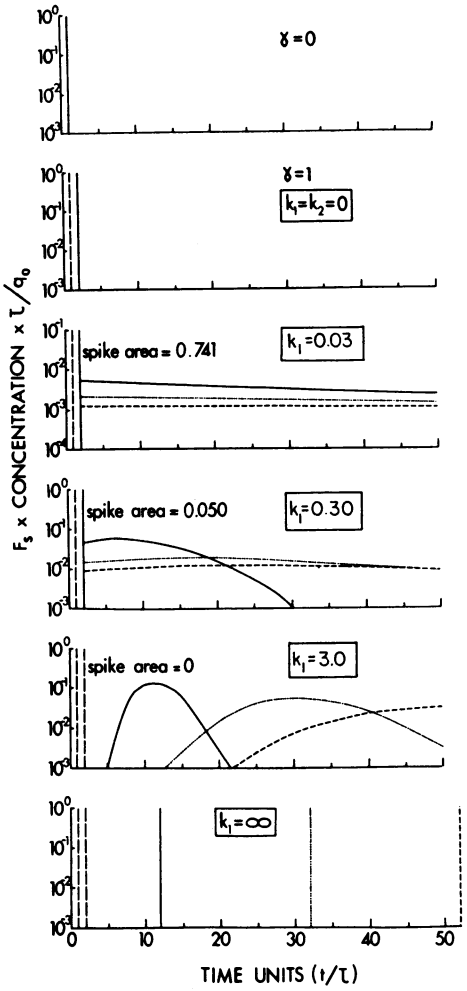

FIGURE 9 Outflow profiles. The profile in the upper panel corresponds to the vascular reference, labeled red cells; that in the second, to the extracellular reference substance; and those in the lower panels, to substances undergoing intracellular transport from the extracellular space. In each instance the input has been an impulse function. For the exchanging substance separate tail functions have been plotted for the k_1/k_2 values 1.0, 3.0, and 5.0 (the corresponding loci are solid, dotted, and dashed). It is difficult to display an impulse function, which theoretically has an infinitely large magnitude and an infinitesimally short duration. In this illustration we have used a vertical line at the appropriate time, and have indicated the associated area by the term spike area, where it differs from unity. It should be noted that the ordinate scale in this illustration is logarithmic.

Outflow response from the whole liver. The terminal vascular bed of the liver is quasicrystalline, from the anatomical point of view. The lengths of the sinusoids in each hepatic lobule are relatively uniform and therefore variations in sinusoidal transit times result from variation in the sinusoidal velocity, W_s. In general (15), one would expect to find a variation in the time spent by the vascular reference substance in both the

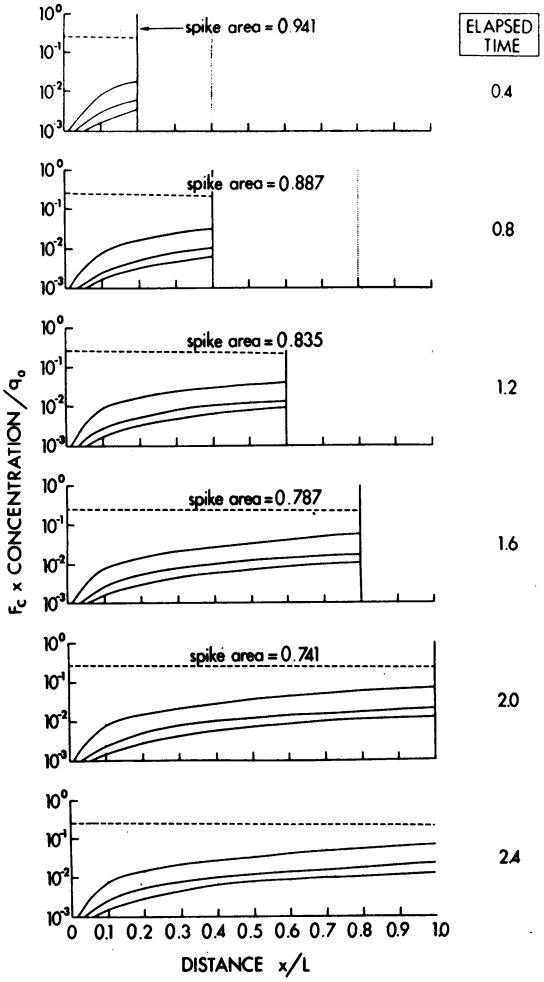

FIGURE 10 Concentration profiles in space. A normalized time scale (t/τ) has been used and the profiles are displayed at normalized time intervals of 0.4. We have once again placed vertical lines at the sites of the impulse functions (that for the red cells is dotted, and that for the diffusible material is solid). The red cell impulse function travels twice as fast as the impulse function associated with the exchanging material, and it emerges at the time interval 1.0. Whereas the red cells are confined to the vascular space, the diffusible material impulse function sweeps along past the cell surfaces in the sinusoidal and extracellular space, an area twice as large. The total amount of material associated with this impulse function is displayed as a "spike area" on the illustrations. Profiles are illustrated for three k_1/k_2 ratio values: 1.0, 3.0, and 5.0. The ordinate scale is logarithmic. With this kind of scale one could not perceive the difference between the intracellular profiles in the three instances being considered and so the virtually common intracellular profile is displayed by use of a single dashed line. The trailing intravascular profile, which extends across the sinusoidal and extracellular space, is displayed as a solid line, in each instance. The magnitudes of the trailing parts of this profile decrease with increase in the ratio k_1/k_2, in each panel.

large (nonexchanging) vessels and the sinusoids (the exchanging vessels). If we define $Q(t)$ = the quantity of material emerging at the outflow per unit time; F = the total flow through the system; $C(t) = Q(t)/F$, the concentration of material appearing at the outflow; $m\left(t_0, \frac{L}{W_s}\right)d\left(\frac{L}{W_s}\right)dt_0$ = the number of sinusoidal pathways with large vessel transit times from t_0 to $t_0 + dt_0$, and with sinusoidal transit times from L/W_s to $L/W_s + d(L/W_s)$; and $qAW_s/F = qF_s/F$ = the proportion of q, the total amount of material injected, which enters a sinusoid with the flow F_s; then

$$C(t) = \frac{1}{F}\int_{t_{0\min}}^{t_0}\int_{(L/W_s)_{\min}}^{L/W_s} \frac{qF_s}{F}\frac{F_s}{q_0}u(L, t - t_0) \times m\left(t_0, \frac{L}{W_s}\right)d\left(\frac{L}{W_s}\right)dt_0. \quad (7)$$

If we assume that there is a functional homogeneity to the perfusion of the liver such that, in any area, the distribution of sinusoidal transit times is independent of the distribution of large vessel transit times, then the double distribution $m\left(t_0, \frac{L}{W_s}\right)d\left(\frac{L}{W_s}\right)dt_0$ may be expressed as the product distribution $r(t_0)n\left(\frac{L}{W_s}\right)d\left(\frac{L}{W_s}\right)dt_0$, where $r(t_0)dt_0$ is the proportion of large vessel transit times from t_0 to $t_0 + dt_0$, and $n\left(\frac{L}{W_s}\right)d\left(\frac{L}{W_s}\right)$ is the proportion of sinusoids with transit times from $\frac{L}{W_s}$ to $\frac{L}{W_s} + d\left(\frac{L}{W_s}\right)$. For the vascular reference substance, then

$$C(t)_{\text{ref}} = \frac{1}{F}\int_{t_{0\min}}^{t_0}\int_{(L/W_s)_{\min}}^{L/W_s}\frac{qF_s}{F} \times \delta\left(t - t_0 - \frac{L}{W_s}\right)r(t_0)n\left(\frac{L}{W_s}\right)d\left(\frac{L}{W_s}\right)dt_0 = \frac{1}{F}\int_{t_{0\min}}^{t_0}\frac{qF_s}{F}r(t_0)n(t - t_0)dt_0.$$

The outflow concentration profile is a convolution integral of the distributions of large vessel and sinusoidal transit times, as expected.

When the hepatic perfusion rate is high, the assumption of regional homogeneity is probably reasonable. When it is low, however, it is not. When the perfusion rate is reduced to values less than 1.5 $ml \cdot min^{-1} \cdot g^{-1}$, the liver blood volume declines with flow (29), and dilution curves carried out on the liver yield grossly bumpy dilution curves (11); and, at very low perfusion rates, a macroscopic heterogeneity in the distribution of labeled water becomes demonstrable (30, 31).

We have, in the past, used the approximation $r(t_0) = \delta(t_0)$ to describe the distribution of large vessel start times in the liver. Whence

$$C(t) = \frac{1}{F}\int_{(L/W_s)_{\min}}^{L/W_s}\frac{qF_s^2}{q_0F}u(L, t - t_0)n\left(\frac{L}{W_s}\right)d\left(\frac{L}{W_s}\right) \quad (7A)$$

The chief past justification for the use of this assumption, the approximation that the large vessel transit times are uniform, is that the resulting model has been shown to accurately describe the progressive change in shape of outflow dilution curves which occurs in the flow-limited case (11), and to provide a fairly precise description of the relation between the outflow dilution curves for labeled albumin and sulfobro-

mophthalein (28). We will continue to use it here. Its current justification is outlined in the discussion section of the manuscript.

Now let us, for convenience in later time scaling, establish a new zero time t_0, and use the new time scale $\tau' = t - t_0$. Then, if we substitute into equation 7A the various "single sinusoidal effects" we find

$$C(\tau')_{\mathrm{RBC}} = \frac{1}{F}\int_{(L/W_s)_{\min}}^{L/W_s} \frac{qF_s}{F}\delta\left(\tau' - \frac{L}{W_s}\right)n\left(\frac{L}{W_s}\right)d\left(\frac{L}{W_s}\right)$$

$$= \frac{1}{F}\cdot\frac{qF_s}{F}n(\tau') \qquad (7B)$$

for the vascular reference substance;

$$C(\tau')_{\mathrm{ec}} = \frac{1}{F}\int_{(L/W_s)_{\min}}^{L/W_s} \frac{qF_s}{F}\delta\left(\tau' - [1 + p\gamma]\frac{L}{W_s}\right) \times n\left(\frac{L}{W_s}\right)d\left(\frac{L}{W_s}\right)$$

$$= \frac{C(\tau'/[1 + p\gamma])_{\mathrm{RBC}}}{(1 + p\gamma)} \qquad (7C)$$

for the extracellular reference substance (32); and

$$C(\tau')_{\mathrm{exch}} = \frac{1}{F}\int_{(L/W_s)_{\min}}^{L/W_s} \frac{qF_s}{F} \times\exp(-k_1\theta\tau')\delta\left(\tau' - [1 + p\gamma]\frac{L}{W_s}\right)n\left(\frac{L}{W_s}\right)d\left(\frac{L}{W_s}\right)$$

$$+ \frac{1}{F}\int_{(L/W_s)_{\min}}^{L/W_s} \frac{qF_s}{F}\exp\left(-\frac{k_2}{r}\tau'\right) \times\exp\left[-\left(k_1\theta - \frac{k_2}{r}[1 + p\gamma]\right)\frac{L}{W_s}\right]\times \sum_{m=1}^{\infty}\frac{\left(k_1\theta\frac{k_2}{r}\frac{L}{W_s}\right)^m\left(\tau' - [1 + p\gamma]\frac{L}{W_s}\right)^{m-1}n\left(\frac{L}{W_s}\right)d\left(\frac{L}{W_s}\right)}{m!(m-1)!}$$

$$= \exp(-k_1\theta\tau')\frac{C(\tau'/[1 + p\gamma])_{\mathrm{RBC}}}{(1 + p\gamma)} + \exp\left(-\frac{k_2}{r}\tau'\right)\int_{(L/W_s)_{\min}}^{L/W_s}\exp\left[-\left(k_1\theta - \frac{k_2}{r}[1 + p\gamma]\right)\frac{L}{W_s}\right]C(\tau')_{\mathrm{RBC}} \times \sum_{m=1}^{\infty}\frac{\left(k_1\theta\frac{k_2}{r}\frac{L}{W_s}\right)^m\left(\tau - [1 + p\gamma]\frac{L}{W_s}\right)^{m-1}d\left(\frac{L}{W_s}\right)}{m!(m-1)!} \qquad (7D)$$

for the exchanging substance. The complete outflow profile for the whole organ is found to also consist of two parts: a first term describing the throughput material, which is sweeping past the surface of the liver cells but which never enters these cells; and a second term, material which has entered the cells and emerged later and which consequently is predominantly spread out in later time, in comparison to the extracellular reference material.

ACKNOWLEDGMENTS

We wish to express our appreciation to Miss Susan Aynsley for her expert technical assistance; and to Miss Margaret Mulherin who, with patience and care, typed this manuscript.

This work was supported by the Medical Research Council of Canada and by the Quebec Heart Foundation.

REFERENCES

1. Robinson, R. A., and R. H. Stokes. 1959. Electrolyte solutions. Butterworth Scientific Publications. London.
2. Tyor, M. P., and J. S. Eldridge. 1956. A comparison of the metabolism of rubidium-86 and potassium-42 following simultaneous injection into man. *Am. J. Med. Sci.* **232**: 186.
3. Burch, G. E., S. A. Threefoot, and C. T. Ray. 1955. The rate of disappearance of Rb^{86} from the plasma, the biologic decay rates of Rb^{86}, and the applicability of Rb^{86} as a tracer of potassium in man with and without chronic congestive heart failure. *J. Lab. Clin. Med.* **45**: 371.
4. Sheehan, R. M., and E. M. Renkin. 1972. Capillary, interstitial and cell membrane barriers to blood-tissue transport of potassium and rubidium in mammalian skeletal muscle. *Circ. Res.* **30**: 588.
5. Relman, A. S., A. T. Lambie, B. A. Burrows, and A. M. Roy. 1957. Cation accumulation by muscle tissue: the displacement of potassium by rubidium and cesium in the living animal. *J. Clin. Invest.* **36**: 1249.
6. Love, W. D., R. B. Romney, and G. E. Burch. 1954. A comparison of the distribution of potassium and exchangeable rubidium in the organs of the dog, using rubidium^{86}. *Circ. Res.* **2**: 112.
7. Goresky, C. A. 1970. The interstitial space in the liver: its partitioning effects. *In* Capillary Permeability. C. Crone and N. A. Lassen, editors. Munksgaard, Copenhagen. 415.
8. Chinard, F. P., G. J. Vosburgh, and T. Enns. 1955. Transcapillary exchange of water and other substances in certain organs of the dog. *Am. J. Physiol.* **183**: 221.
9. Friedman, J. J. 1968. Muscle blood flow and ^{86}Rb extraction: ^{86}Rb as a capillary flow indicator. *Am. J. Physiol.* **214**: 488.
10. Goresky, C. A. 1967. The distribution of substances in a flow-limited organ, the liver. *In* Compartments, Pools, and Spaces in Medical Physiology. P.-E. Bergner, C. C. Lushbaugh, and E. Anderson, editors. Oak Ridge Institute for Nuclear Sciences Symposium. Division of Technical Services of the U. S. Atomic Energy Commission. 423.
11. Goresky, C. A. 1963. A linear method for determining liver sinusoidal and extravascular volumes. *Am. J. Physiol.* **204**: 626.
12. Shoemaker, W. C., W. F. Walker, T. B. Van Itallie, and F. D. Moore. 1959. A method for simultaneous catheterization of major hepatic vessels in a chronic canine preparation. *Am. J. Physiol.* **196**: 311.

13. Hamilton, W. F., J. W. Moore, J. M. Kinsman, and R. G. Spurling. 1928. Simultaneous determination of the pulmonary and systemic circulation times in man and of a figure related to the cardiac output. *Am. J. Physiol.* **84**: 338.
14. Zierler, K. L. 1964. Basic aspects of kinetic theory as applied to tracer distribution studies. *In* Dynamical Clinical Studies with Radioisotopes. U. S. Atomic Energy Commission, Division of Technical Information, Oak Ridge, Tenn. 55.
15. Sheppard, C. W. 1954. Mathematical considerations of indicator dilution techniques. *Minn. Med.* **37**: 93.
16. Bassingthwaighte, J. B., F. H. Ackerman, and E. H. Wood. 1966. Applications of lagged normal density curve as a model for arterial dilution curves. *Circ. Res.* **18**: 398.
17. Thompson, H. K., C. F. Starmer, R. E. Whalen, and H. D. MacIntosh. 1964. Indicator transit time considered as a gamma variate. *Circ. Res.* **14**: 502.
18. Goresky, C. A., and M. Silverman. 1964. Effect of correction of catheter distortion on calculated liver sinusoidal volumes. *Am. J. Physiol.* **207**: 883.
19. Levitt, D. G. 1971. Theoretical model of capillary exchange incorporating interactions between the capillaries. *Am. J. Physiol.* **220**: 250.
20. Perl, W., and F. P. Chinard. 1968. A convection-diffusion model of indicator transport through an organ. *Circ. Res.* **22**: 273.
21. Bassingthwaighte, J. B., T. J. Knopp, and J. B. Hazelrig. 1970. A concurrent flow model for capillary-tissue exchange. *In* Capillary Permeability. C. Crone and N. A. Lassen, editors. Munksgaard, Copenhagen. 60.
22. Renkin, E. M. 1959. Transport of potassium-42 from blood to tissue in isolated mammalian skeletal muscles. *Am. J. Physiol.* **197**: 1205.
23. Crone, C. 1963. The permeability of capillaries in various organs as determined by the "indicator diffusion" method. *Acta Physiol. Scand.* **58**: 292.
24. Goresky, C. A., W. H. Ziegler, and G. G. Bach. 1970. Capillary exchange modeling: barrier-limited and flow-limited distribution. *Circ. Res.* **27**: 739.
25. Goresky, C. A. 1964. Initial distribution and rate of uptake of sulfobromophthalein in the liver. *Am. J. Physiol.* **207**: 13.
26. Prothero, J., and A. C. Burton. 1961. The physics of blood flow in capillaries. I. The nature of the motion. *Biophys. J.* **1**: 565.
27. Goresky, C. A., R. F. P. Cronin, and B. E. Wangel. 1969. Indicator dilution measurements of extravascular water in the lungs. *J. Clin. Invest.* **48**: 487.
28. Levi, A. J., Z. Gaitmaitan, and I. M. Arias. 1969. Two hepatic cytoplasmic protein fractions, Y and Z, and their possible role in the hepatic uptake of bilirubin, sulfobromophthalein, and other organic anions. *J. Clin. Invest.* **48**: 2156.
29. Brauer, R. W. 1963. Liver circulation and function. *Physiological Reviews.* **43**: 115.
30. Griffin, W. O., Jr., D. G. Levitt, C. J. Ellis, and N. Lifson. 1970. Intrahepatic distribution of hepatic blood flow: single-input studies. *Am. J. Physiol.* **218**: 1474.
31. Lifson, N., D. G. Levitt, W. O. Griffin, Jr., and C. J. Ellis. 1970. Intrahepatic distribution of hepatic blood flow: double-input studies. *Am. J. Physiol.* **218**: 1480.
32. Goresky, C. A., and G. G. Bach. 1970. Membrane transport and the hepatic circulation *Ann. N. Y. Acad. Sci.* **170**: 18